Title

X-ray Computed Microtomography: A Non-invasive and Time-efficient Method for Identifying and Screening Roman Copper-based Coins

Authors: Francesco Abate,[a,b] Michela De Bernardin,[a] Maria Stratigaki,[a] Giulia Franceschin,[a] Fauzia Albertin,[c] Matteo Bettuzzi,[d] Rosa Brancaccio,[d] Anita Bressan,[e] Maria Pia Morigi,[d] Salvatore Daniele,[b] Arianna Traviglia[a*]

[a] Center for Cultural Heritage Technology (CCHT@Ca'Foscari), Istituto Italiano di Tecnologia, Via Torino 155, 30172 Venezia (Italia). E-mails: francesco.abate@iit.it, michela.debernardin@iit.it, maria.stratigaki@iit.it, giulia.franceschin@iit.it, (*)arianna.traviglia@iit.it

[b] Department of Molecular Sciences and Nanosystems, Università Ca' Foscari Venezia, Via Torino 155, 30172 Venezia (Italia). E-mail: sig@unive.it

[c] Istituto di Scienze e Tecnologie Chimiche 'Giulio Natta', SCITEC – CNR, Via Elce di Sotto 8, 06123 Perugia (Italia). E-mail: fauzia.albertin@scitec.cnr.it

[d] Department of Physics and Astronomy 'Augusto Righi', Università di Bologna, Viale Berti Pichat 6/2, 40127 Bologna (Italia). E-mails: matteo.bettuzzi@unibo.it, rosa.brancaccio@unibo.it, mariapia.morigi@unibo.it

[e] Freelance conservator, Via della Resistenza 8, 30033 Noale (Venezia, Italia). E-mail: anita.bress@gmail.com

Abstract

This study utilises X-ray Computed Micro-Tomography (µXCT) as a non-destructive and non-invasive method to recover the original surface features and reveal the characteristics of encrusted, illegible Roman copper-based coins before any physical cleaning process is performed. The coins were retrieved from the topsoil during an archaeological survey in the countryside of the ancient city of Aquileia, Italy, and were severely degraded, covered with accumulated matter and pronounced encrustations developed over centuries of aging buried in soil. Despite their condition, most of the coins were identified from a numismatic standpoint using tomographic data alone, with the aid of reference images. They were subsequently cleaned using traditional manual methods and the results compared with µXCT. X-ray Fluorescence (XRF) analysis of the coins after the physical cleaning confirmed their numismatic attribution and revealed information regarding the influence of different alloy compositions on the applicability of the µXCT method, as well as on the corrosion process of the coins.

This study showcases how the application of µXCT on fragile corroded metal artifacts prior to any intrusive manual procedures can expedite the identification process, mitigating the risk of information loss caused by physical handling and cleaning. This approach proves particularly valuable when dealing with large numbers of coins that would typically require restoration for identification purposes. It also emphasises the numerous advantages of using µXCT for coin identification, provenance determination, dating, virtual restoration, digitisation, and long-term preservation.

Keywords: Archaeology, Roman, copper, coins, X-ray computed tomography, numismatics

1 Introduction

Ancient coins are a primary source for understanding the human past, as they provide invaluable information about the economy, politics, and society of the time [1–3]. To be used as a source of documentation, coins must be correctly identified from a numismatic perspective. This involves analysing various aspects of the coin, such as its size, weight, shape, inscriptions, symbols, and images, in order to determine its origin, date of production, and the historical context in which it was produced and used. Without proper numismatic identification, the historical significance of a coin may be lost or misinterpreted, making it less useful as a means of acquiring relevant knowledge.

Coins that are discovered in direct contact with soil are often in a compromised state of conservation [4,5]. Long-lasting exposure to burial conditions can cause them to deteriorate due to the interactions with the surrounding environment. This can lead to the development of thick *patina*s and pronounced encrustations of soil on their surfaces, making their identification challenging [6,7].

After being discovered, coins may undergo one or more treatments to recover numismatic information, each with potential consequences. Coins are usually subjected to an initial superficial cleaning just after their recovery, to remove surface soil and allow for a quick screening [8]. However, this preliminary physical cleaning process may fail to retrieve residual surface details, leaving significant information hidden. In some cases, it may even lead to an irreversible loss of important details [9–12], or cause additional degradation of the bulk metal. For instance, this can happen to copper coins due to the occurrence of bronze disease, which can be triggered by the direct exposure to environmental oxygen of copper chlorides that may be concealed inside or beneath corrosion *patina* and encrustations [13,14]. Less frequently, coins undergo micro-excavation and cleaning operations in laboratory settings by hand of restorers [15]. However, this approach is time-consuming and not practical for large numbers of copper coins [15–18] to such an extent that often only coins intended for display in museum exhibits are cleaned and restored, while the rest remain stored away in their state of recovery or only partially cleaned, unable to reveal the information they hold [19].

This scenario calls for a time-efficient, non-invasive method for coin identification that can protect against the loss of valuable information during physical cleaning and facilitate the examination of coins on a comprehensive scale. In this regard, several studies have been conducted to test remote recognition methods for coins using X-ray Computed Microtomography (μXCT) [6,7,20–26]. This technique is widely acknowledged for its powerful capability in revealing hidden features, its mature technology, widespread deployment, and non-invasive nature, making it a valuable tool in various fields of research. In particular, μXCT has been utilised to support the identification of uncleaned silver [20–24] and, to a minor extent, copper coins [6,7,25,26]. However, there is currently a lack of direct comparison between μXCT and traditional cleaning methods, which introduces uncertainty regarding the degree of equivalence or difference in the outcomes of these two types of approaches. A comprehensive comparison needs to be conducted to evaluate the specific reduction in identification times compared to cleaning practises. Additionally, μXCT has mainly been applied to individual objects and has not been tested on a large scale, making it unclear whether the method is suitable across the broad spectrum of Roman copper coinage.

To systematically explore the potential of μXCT in identifying Roman copper-based coins, an investigation was conducted to compare the results obtained from μXCT scans of corroded and soil-encrusted coins with those obtained through manual cleaning. Eleven coins were initially scanned by μXCT in their recovery state to enable their identification by a numismatist. Subsequently, they underwent a cleaning

phase by hand of a restorer. One additional coin, which was mechanically cleaned prior to this study, was scanned by µXCT once cleaned. Finally, all the cleaned objects were analysed using X-ray Fluorescence to confirm the attribution of coin types and assess the influence of the latter on the applicability of our method and the conservation state of the coins. The findings of this study reveal that µXCT surpasses traditional cleaning methods and indicate that the technique should be actively integrated into archaeological and numismatic practice.

2   Research aim

The primary aim of this research was to determine the extent of improvement that can be achieved by µXCT in the recognition and attribution of illegible ancient coins – that retain soil or other debris encrustations or have undergone corrosion – over traditional cleaning procedures.

In pursuit of this, the study aimed to accomplish the following objectives: to evaluate the limitations and challenges associated with invasive and time-consuming cleaning methods typically employed for large coin collections; to assess the potential damage caused by traditional cleaning methods and the subsequent loss of valuable information; to define a non-invasive procedure for the identification of large numbers of coins based on µXCT; to assess the benefits of this procedure and to define its range of applicability within the Roman copper coinage domain.

By successfully fulfilling these objectives, this research sought to provide valuable insights and recommendations for the integration of µXCT into coin identification practices, thereby improving the overall management and preservation protocols of numismatic collections.

3   Materials and Methods

3.1   Coins description

The analysis was conducted on a set of 12 Roman copper-based coins, which had been recovered in the vicinity of ancient Aquileia (Italy) during archaeological fieldwalking surveys. A visual inspection of coins in their as-found conditions revealed compromised and poor conservation states, with surfaces bearing greenish malachite-like *patinas*, typical green-red *patina*s associated with the presence of malachite and cuprite, encrustations with vivid blue or orange shades, and powdery deposits of dirt, as well as thick crusts of soil and accumulated matter. Complete documentation of the coins is shown in Tables S1 as well as Figures S1, S2, and S3.

3.2   µXCT: set-up

The µXCT analysis was conducted using a custom-made system assembled by the hosting group in Università di Bologna. The system is composed by a rotating stage, a Hamamatsu L12161-07 75W microfocus X-ray tube with a spot size of 20 µm and a Varian PAX SCAN 2520D flat-panel detector with 1536 horizontal and 1920 vertical pixels, each measuring 127x127 µm², resulting in a total effective area of 19.5 x 24.3 cm². The voltage applied was 150 kV, the maximum for this system, with a current ranging between 140 and 180 µA. To minimise Beam Hardening (BH) effects (SI, Appendix A), different filters (1

mm Al, 0.1 mm Cu, 0.25 mm Pb plus 0.1 mm Cu) were applied to the incident beam. For each scan, approximately 1 hour was required to capture 900 radiographies over 360° in step mode, with each radiography obtained as a mean over 4 repeated acquisitions taken at the same angular position, at a rate ranging from 5 to 3 frames per second. To achieve a voxel of 40 µm side, a magnification of x3.18 was used during the scans.

The choice of the number of radiographic projections and of the level of magnification were based on a time-optimisation criterion. The number of projections should at least equal the number of pixels in the horizontal direction, in order not to decrease resolution in regions far from the center of rotation [27,28]. Due to their size and to the x3.18 magnification adopted, the coins occupied at most ca. half of the horizontal pixels of the detector. On these bases, the number of 900 projections was considered as an optimal compromise. While the µXCT system used would have allowed a further increase in the level of magnification, in fact, it would have determined an increase in the number of projections required and in the final data size, negatively affecting the total acquisition and elaboration time.

Each µXCT scan involved 2 to 3 coins, kept still in vertical alignment by two blocks of polystyrene. The total number of coins that could be scanned per time was determined by the combination of detector effective area, level of magnification and coins size. The vertical alignment was chosen in order to avoid the overlapping of multiple coins along the beam direction, which would cause an increase of the path length of X-rays inside metallic bulk and thus an excess of beam absorption and enhanced beam hardening effects, overall worsening the quality of XCT data.

The CT reconstruction was carried out using the Feldkamp algorithm for cone beam CT [29], which is based on filtered−back projection (FBP) [27]. The PARREC (PARallel REConstruction) software was utilised for this purpose. [30–32]. The volume reconstruction of a single scan, which included 2-3 coins, was done simultaneously with the scanning process on a separate computer and was completed in less than an hour.

3.3   µXCT: data analysis, processing, interpretation

The µXCT data underwent a post-processing correction algorithm to address BH artefacts. The reconstructed datacubes were then processed using open-source software ImageJ [33] and 3DSlicer [34]. A detailed description of data processing steps is reported in the Supporting Information (Appendix A and Appendix B). The identification of coins was conducted using the processed data, with an archaeologist specialised in numismatics referencing up-to-date catalogues and repositories [35–38].

3.4   Traditional cleaning of coins

The coins were cleaned by a professional restorer who followed a standard workflow for manual, basic cleaning, using simple tools such as a scalpel, dental probes, pins, and synthetic brushes instead of more sophisticated laboratory equipment. Ethanol and acetone were used as softening agents to remove soil crusts, but no chelating agents were used due to the poor condition of the coins. The entire process was carried out under a magnifying lens to ensure accuracy of the cleaning intervention, and it took approximately one working day to clean each coin. Details regarding the weight and thickness of the coins after cleaning are provided in Tab. S1.

3.5 XRF elemental analysis

The XRF analysis was conducted on the cleaned coins using a Bruker Crono instrument, which included a Rh-target 10W X-ray tube, a 1 mm collimator, and an XFlash® detector. The instrument operated at 50 kV and 200 µA, with a total acquisition time of 60 seconds. To account for local inhomogeneities, measurements were taken in triplicate for both sides of each coin by varying the position. The spectral elaboration and quantification were performed using Bruker ESPRIT® (v2.2) software, while statistical analysis was carried out using RStudio 1.4 [39].

4 Results & Discussion

4.1 Identification of coins *via* µXCT

The 12 coins analysed via µXCT were classified into different groups based on the level of identification achieved. Group A (Fig. 1) includes five coins that were fully identified, while Group B (Fig. S1) comprises five coins that were partially identified. One coin was illegible and placed in Group C (Fig. S2), while Group D (Fig. S3) consists of one coin that was cleaned before undergoing µXCT scanning. For each coin, a numismatic interpretation based on the tomographic data is provided, along with a comparison of the results obtained through traditional cleaning methods.

4.1.1 Group A - Complete identification

Five coins were successfully identified using µXCT. Reconstructed volumes and 3D rendering techniques based on tomographic data allowed for the determination not only of the numismatic type, but also of the specific coin issue through comparison with reference coins from online repositories. Fig. 1 displays images of the coins as they were retrieved from the archaeological site and compares the results obtained from traditional cleaning and µXCT, along with the reference images used for identification. It is evident that the µXCT data provided a much higher level of detail of the original surface that was still preserved beneath or within the corrosion layers, thereby facilitating coin identification.

In the case of coin A1, the analysis revealed the well-preserved profile of *Maximianus Herculius* under layers of accumulated matter and corrosion. The coin has been identified as a proper *follis* issued by the Imperial mint of *Tincinum* (modern Pavia, in Italy) in 300-303 CE or in 304-305 CE. The obverse side shows the laureate head of the emperor facing right, while the reverse side depicts *dea Moneta* (goddess of Mint) standing, facing left, holding scales with the right hand and *cornucopiae* on the left arm. Results obtained after the cleaning process are consistent with those from the µXCT analysis only for the obverse side of the coin, displaying the recognisable profile of *Maximianus* with some letters. On the reverse side, however, no traces of the female figure or of the legend found in the tomographic reconstruction can be discerned after cleaning.

Coin A2 presented a thick layer of dirt and corrosion on both sides, with a portion on the upper part presumably already detached when it was found on site. Nonetheless, µXCT supported the identification of the coin as an *antoninianus* issued by Valerian I (257-259 CE, mint of *Mediolanum*). On the obverse, the radiate, draped bust of the emperor Valerian I facing right can be observed, while, on the reverse side, *dea Salus* (goddess of Health) appears draped, standing facing right and feeding a serpent held in her arms. The cleaned coin, on the other hand, is scarcely legible on the obverse side, as only traces of a

radiate head can be seen. On the reverse side, *Salus* figure can be discerned. Therefore, the coin is only partially readable after cleaning.

Figure 1 Group A: five coins completely identified using μXCT. Images of coins correspond to: as retrieved from the excavation site, after cleaning, after 3D rendering based on tomographic reconstructions, and reference images from online repository (with the permission of wildwinds.com [40]). Obverse (obv in figure) and reverse (rev) sides are provided for each coin. Images are not to scale. Full reference data are provided in Tab. S2.

The tomographic reconstruction performed on coin A3 revealed the head of *Caesar Crispus*, son of emperor Constantine I, on the obverse side. The coin is identifiable as a small bronze (AE3, *nummus*)

issued by the mint of Arles (317 CE) bearing the laureate, draped, and cuirassed bust of the young Caesar facing right on the obverse. On the reverse, the god Mars is standing on the right in military dress, with a coat across the left shoulder, leaning on the shield, and holding a vertical spear, reversed. After physical cleaning, the legibility of the coin is still minimal due to its degraded conservation state, which further led to a small portion of the *patina* being detached on the obverse. Two letters ('C R', i.e., the beginning of the name *Crispus*) and a detail of the laurel crown were revealed via μXCT in the area affected by the detachment, while after cleaning only a faint mark of the latter was visible. On the reverse, instead, only Mars' spear is distinguishable.

Coin A4 is identified after the μXCT analysis as a small bronze (AE3, *nummus*) of Constans I issued between 337 and 341 CE in *Siscia* (modern Sisak, Croatia). It displays the bust of the emperor with a rosette diadem, draped, and cuirassed facing right on the obverse. On the reverse, two soldiers holding spears and shields flank a standard, with the Chi-Rho on the banner. In particular, the mark on the banner was initially identified as an O mark. After the application of a band-pass filter, the Chi-Rho mark became clearly visible (Fig. 2), allowing a shift in the dating of the object from 346-348 CE back to a decade earlier. After the cleaning process, the coin shows the faint profile of an emperor with a rosette diadem: the letters 'CON' are visible as well as scarce traces of 'TA' (i.e. the remnants of the name *Constans*). On the reverse, the corrosion makes almost every detail of the struck surface indiscernible. Only the relief of the two soldiers is still recognisable.
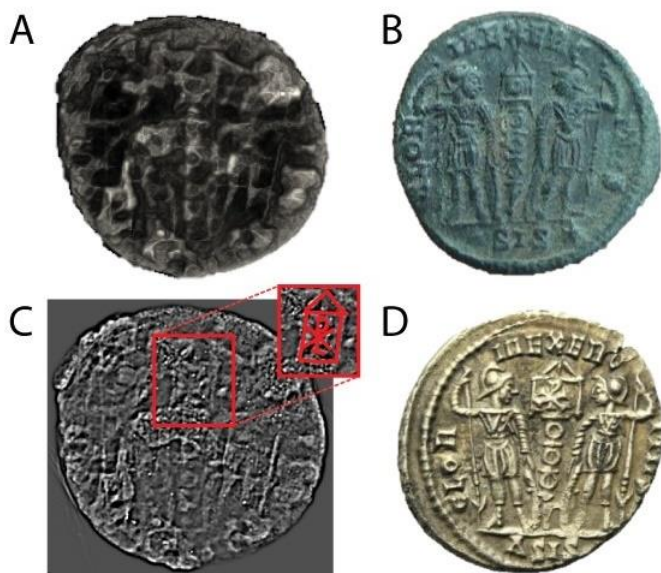

Figure 2 Coin A4: (A) 3D rendering and (B) related identification based on unfiltered μXCT data. (C) Reconstructed slice after the application of a low-pass filter, with the 'Chi-Rho' mark highlighted in red. (D) Final identification.

Despite the apparently poor condition of coin A5, μXCT revealed the fine profile of emperor Severus Alexander. The coin can be identified as a *denarius* issued by the young ruler in 229 CE in Rome. On the obverse, it shows the laureate head of the emperor facing right. On the reverse, there is the god Mars helmeted, walking left, holding an olive branch in the right hand, and a spear and shield in the left. Coin A5 is the only one that proved to be almost as identifiable after the traditional cleaning. Fig. 3 portrays the obverse side of coin A5, and compares the results achieved by μXCT and cleaning. It is evident that the level of details of the lettering is finer and more precise on the XCT-based rendering. Furthermore,

during the physical cleaning, a small portion of the legend was detached, revealing a silvered but flat surface in the area where the letters 'XA' and part of the letter 'N' (i.e. the remnants of the name *Alexander*) were visible in the 3D rendering.
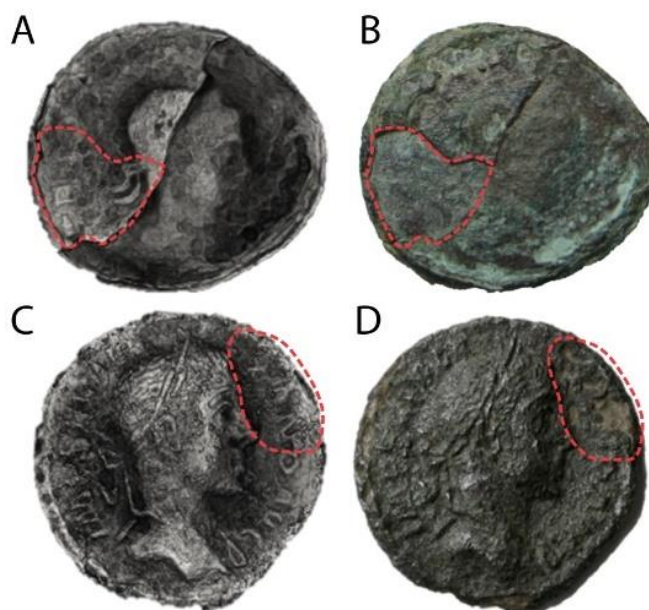

Figure 3 Comparison of the XCT-based 3D rendering and photo after traditional cleaning for the obverse side of coins A3 (A: 3D rendering; B: photo) and A5 (C: 3D rendering; D: photo). The flakes fallen off during cleaning phase are highlighted in red.

4.1.2   Group B - Partial identification

Figure S1 summarises the results of the five coins where μXCT has successfully retrieved all surviving details of the original surface, but it was not sufficient for a complete identification of the coins. μXCT allowed to distinguish between the obverse and reverse sides, revealing faint traces of the head profiles of issuing emperors, two radiate (B1, B2), two laureate (B3, B4), and one not discernible (B5). In three instances, glimpses of a standing figure on the reverse were visible, two male (B2, B3) and one female (B1). The reverse of B4 remained illegible. On the reverse of coin B5, an 'S' mark is visible, oddly appearing as a hollow cavity. Overall, the metrology and the partial details provided by μXCT allowed for hypothetical identification as two small bronze denominations (AE3) possibly from the 4th century (B2, B4), an *antoninianus* possibly from the mid-3rd century (B1), and two Imperial *asses* (B3 and B5), the first of which might be attributed to a Flavian emperor based on the profile emerged with the μXCT. All coins in Group B displayed features after cleaning that are comparable to the ones observed on the virtually restored ones.

4.1.3   Group C and D

Coin C, tentatively identified as a Republican *as* according to numismatic evaluation, showed no visible signs of the original surface under μXCT (Fig. S2) due to severe beam hardening effects. Nevertheless, the coin showed a completely worn surface after the cleaning process, most likely due to severe corrosion.

Unlike the other coins analysed in this work, Coin D has been subjected to a physical cleaning prior to μXCT scanning, without any success in retrieving useful information for its identification. The tomographic

reconstruction revealed the presence of the letters 'S C' (Fig. 4) presumably standing for *'Senatus Consultum'*, interpreted as a hint to the authority acknowledged to the Roman Senate over the minting of copper-based coinage. This mark was commonly present on the reverse side of copper-alloy coins until the period of *Diocletianus* (ca. 294 CE) [41,42].
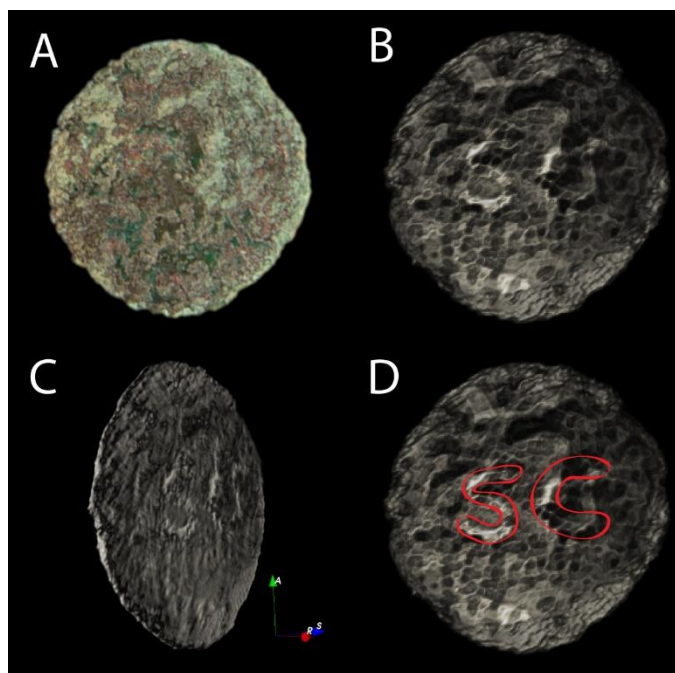

Figure 4 (A) Coin D. (B) Single slice from the tomographic reconstruction. (C) 3D rendering based on tomographic data (D) 'S C' mark highlighted in red on top of figure 4B.

4.2 Verification of coin denomination through alloy composition analysis using XRF

The XRF analysis was performed after the physical cleaning to confirm the identification of the coins in terms of typology. While XRF is commonly used to estimate the elemental composition of materials, the presence of thick alteration layers and accumulated matter on corroded ancient coins makes it challenging to achieve precise quantification of the bulk composition [43]. Therefore, in this context, the XRF data have been treated as semi-quantitative information regarding the constituent material of the coins. Complete results are provided in Tab. S3. As expected, Cu was found to be the primary component in all the coins, with a content varying from 46 to 97 wt.%. The significant presence of common alloying agents for Roman copper coins, such as Ag, Sn, and Pb, was attested in most coins. Zn, on the other hand, was found only in one coin as a trace element. Contamination from soil elements (Mg, Al, Si, Mn, P) was observed in all the analysed coins [20]. A small amount of Cl was detected only on coin A3, locally reaching 1.7 wt.%. The surface of this coin after cleaning presents a powdery pale green corrosion product diffused on both sides, but more concentrated in some areas, suggesting an ongoing bronze disease process.

The XRF data confirm the identification of coin types as indicated by tomographic reconstructions and numismatic evaluation. As expected from their presumed numismatic type, coins A2 (*antoninianus*) and A5 (*denarius*) show a high proportion of silver in the alloy [44,45], whereas coins A3, A4 (two *nummi*), and

A1 (a *follis*) only contain minimal amounts of silver, but significant amounts of tin and lead [41,45–50]. The lower amount of Ag for coin B1 suggests that it could belong to a late *antoninianus* [44], which is consistent with the numismatist's evaluation. The presence of lead and tin in coin C supports its identification as a Republican *as* [51,52]. The binary Cu-Pb and ternary Cu-Sn-Pb (with traces of Ag) alloys of coins B4 and B2, respectively, are compatible with 4th-century *nummi* from different periods [41,44,46–48], while the lack of alloying agents in coins B3 and B5 is typical of Imperial *asses* [45,53]. Coin D appears to be made of pure copper, which, together with the 'S C' mark and the metrology, suggests its identification as a fraction of the *as* of the Imperial era. The absence of zinc, traditionally linked to *sestertii*, further supports the proposed interpretation of the coin types.

4.3 Effect of Pb content and coin thickness

Despite the reports on the effect of Pb on the identification process [6], in this work it appears that its sole presence, in amounts compatible with Roman coinage, does not represent a limiting factor. In fact, all coins of Group A have been identified despite the presence of Pb up to 26 wt.%. It should be noted that XRF on corroded coins tends to overestimate Pb content [43] and literature data for coins similar to A1 report a range of values from 1 to 10 wt.% [50]. However, when a high content of Pb is coupled with increased coin thickness, the readability appears to be hindered. This is the case with coin C, for which the tomographic reconstruction showed a low level of readability due to high absorption effects and consequent low counting of transmitted photons, which also limited the a posteriori correction of beam hardening. Coin C is an alleged Republican *as*, i.e., a class of coins that usually presents a high thickness (5 mm) and a significant Pb content [51–53]. On the other hand, coins that exhibit only a high thickness with no significant Pb content (Imperial *asses*, coins B3 and B5) have been reconstructed via µXCT without issues. It is important to note that 3rd-century *nummi* and late *antoninianii* fall well within the range of applicability of µXCT. This is particularly important to note since the majority of large hoards of ancient Roman copper-based coins are comprised of *nummi* and *antoninianii* [54,55].

It is clear that the readability of a coin is affected only when a high absorbing element such as Pb is present along with a significant object thickness. However, the effects of high absorbing coins can be mitigated by using high-energy X-ray sources that increase the number of transmitted photons [10]. Although we successfully applied our identification method to the most common Roman copper-based coin typologies using a standard 150 kV setup, the use of dedicated high-energy systems can broaden the applicability of the method to include all remaining typologies. µXCT setups with high-energy source are available both commercially as lab-based instruments [23], and in specific synchrotron beamlines [56]. Although synchrotron-based µXCT represents a less accessible option, it can boast a high level of resolution, potentially addressing the requirements of individual challenging cases.

4.4 Effect of Ag content

A correlation between the material of the coins and the preservation state of their original surface can be observed. The coins that have silver in their composition appear to be in a better state of preservation. This may seem obvious for Ag-rich coins, such as coins A2 and A5. However, for the other three coins of group A, we can hypothesise that their preservation is due to the mechanism of Type I *patinas* in copper-tin alloys, as defined by Robbiola et al. (1998). This process involves the formation of a semi-protective inner layer consisting of tin compounds, which effectively controls the ongoing corrosion of objects over extended periods. As a result, it facilitates the enhanced preservation of surface details. In copper-tin alloys, this mechanism typically does not occur in aggressive environments, like the lagoon, due to the

fast initial dissolution rate of copper. Silver, on the other hand, can play a similar role to tin but form stable compounds even in aggressive environments. The formation of a layer of silver compounds, such as Ag_2O or $AgCl$, can mediate the ion flux inward and outward [57,58], slowing down the overall corrosion process and resulting in better preserved surface morphologies of copper-based silver-containing coins. Additionally, silver may be more concentrated near the original surface due to selective dissolution of copper [57], or due to artificial surface enrichment typical for these class of coins [58–62]. Thanks to its natural resistance to corrosion, a local enrichment of silver may enhance its effect on the preservation of the original surface morphology. This may also facilitate the identification of the coins due to the higher contrast that silver provides under X-ray irradiation.

4.5   Corrosion *patina* and bronze disease

The analysis of the tomographic data, supported by 3D renderings and post-cleaning documentation, suggests that the information necessary for coin identification is often stored within the corrosion *patina*, rather than on the surface of the residual bulk metal. For example, the observed side of coin B5 exhibits a corrosion *patina* with a thickness similar to that of the residual bulk. Within that *patina*, some details can be discerned, while the bulk metal only exhibits a completely worn surface.

This phenomenon may be due to X-ray absorption contrast arising from a concentration step in metal ions at a certain position within the *patina* [26]. This position may correspond to the interface between the secondary *patina*, formed by the re-deposition of outward-diffusing metal ions mixed with soil compounds, and the primary *patina*, constituted by in-place oxidised metal atoms and inward-diffusing anions from the environments. The topology of this interface, which barely corresponds in position to the original surface of the coin, may hold memory of the latter and thus reveal the stored information under X-ray tomography.

The tomographic analysis of coin D does not provide a clear indication of whether the information necessary for identification is preserved within the *patina* or on top of the residual bulk. In the latter case, the original metallic surface may not have been completely disrupted by the corrosion process and could be covered by a layer of secondary corrosion products that are both smooth enough to obscure the details of the original surface (such as the 'S C' mark) and compact enough to resist removal during the cleaning process. Similar observations have been previously reported as a deviation from the Type I *patina* [57]. Without any visible signs of residual original surface details, the cleaning of the coin was stopped to prevent any risk to its structural integrity. However, the use of μXCT allowed us to retrieve the hidden information easily and without any risk.

It is important to note that some corrosion *patina*s of copper objects are brittle, poorly adherent, and can be easily fragmented under mechanical stress. Invasive manipulation of copper coins can pose significant risks to their structural integrity. This was demonstrated in the case of coins A3 and A5, where the removal of corrosion flakes resulted in the loss of lettering details and poor legibility (as shown in Fig. 3). However, the use of tomographic data acquired before cleaning allowed us to retrieve and digitally preserve this information.

The effectiveness of μXCT in identifying coins is further highlighted in cases where traditional cleaning methods cannot be used due to the presence of *bronze disease*. The topological information stored within the affected zones may be lost due to invasive cleaning and resulting mechanical stress. Bronze disease by-products, mainly hydroxychlorides, are decoherent and can be easily removed during cleaning, as seen

in the case of coin A3. After cleaning, the coin shows a pale green vacancy where a well-defined figure of a soldier was previously visible in the μXCT scan of the reverse side (Fig. 5). Furthermore, the application of μXCT allows for the postponement of the exposure of active compounds to environmental oxygen and moisture, thereby delaying the re-activation of the autocatalytic decaying process. This provides an opportunity for off-site stabilisation treatment to be undertaken immediately, thus preserving the integrity of the coin.

Figure 5 Reverse side of coin A3 (A) before cleaning, (B) virtually cleaned with μXCT and (C) after traditional cleaning. The loss of most of the figure of a soldier after the invasive cleaning is evident.

5   Conclusions

This study showcases the effectiveness of μXCT in archaeological practice and numismatic research for the rapid and non-invasive identification of unprocessed copper-based Roman coins, eliminating the need for manual cleaning. The results demonstrate that μXCT can retrieve as much information from corroded coins as physical cleaning, while surpassing traditional cleaning methods in terms of identifying the numismatic type of the coins and improving time-efficiency.

The findings indicate that μXCT is applicable for the digital restoration and identification of common types of copper-based Roman coins, including *nummi, antoninianii, denarii, folles,* and Imperial *asses*. Furthermore, the research highlights the risks associated with physical cleaning, such as the removal of information-bearing *patina* and corrosion by-products, emphasising the importance of a non-invasive identification process prior to any invasive intervention. A correlation between the presence of small amounts of silver and the better state of conservation of copper coins has also been observed and explained in terms of corrosion mechanisms.

The proposed method offers numerous advantages in the study and management of ancient coins. By scanning collections of uncleaned coins, it significantly reduces the time required for their identification, addressing the long-standing challenge of large-scale coin analysis. It eliminates the need for physical cleaning, reducing the risk of irreversible damage and loss of information. Even in cases where cleaning is necessary, the approach minimises potential damage by providing digital preservation of information and guiding restorers in the practice of the micro-excavation of coins. Additionally, the use of μXCT enables 3D digitisation of the coins, creating virtual replicas that can be included in online repositories and used for scientific dissemination.

Overall, μXCT scanning is a powerful tool that has the potential to facilitate and promote the study and preservation of coins, with broader implications for archaeological practices and beyond.

6 Acknowledgments

7 Declaration of interest

The authors have no competing interests to declare.

8 Data statement

The datasets generated during the current study are available from the corresponding author.

9 References

[1] P.J. Casey, R. Reece, Coins and the Archaeologist, Seaby, 1988.

[2] C.J. Howgego, Ancient history from coins, Routledge, London ; New York, 1995.

[3] C. Rowan, From Caesar to Augustus (c. 49 BC–AD 14): Using Coins as Sources, Cambridge University Press, 2018. https://doi.org/10.1017/9781139775311.

[4] L. Pronti, A.C. Felici, M. Alesiani, O. Tarquini, M.P. Bracciale, M.L. Santarelli, G. Pardini, M. Piacentini, Characterisation of corrosion layers formed under burial environment of copper-based Greek and Roman coins from Pompeii, Appl. Phys. A. 121 (2015) 59–68. https://doi.org/10.1007/s00339-015-9351-5.

[5] B. Bakirov, I. Saprykina, S. Kichanov, R. Mimokhod, N. Sudarev, D. Kozlenko, Phase Composition and Its Spatial Distribution in Antique Copper Coins: Neutron Tomography and Diffraction Studies, Journal of Imaging. 7 (2021) 129. https://doi.org/10.3390/jimaging7080129.

[6] H.-Y. Nguyen, S. Keating, G. Bevan, A. Gabov, M. Daymond, B. Schillinger, A. Murray, Seeing through Corrosion: Using Micro-focus X-ray Computed Tomography and Neutron Computed Tomography to Digitally "Clean" Ancient Bronze Coins, MRS Online Proceedings Library. 1319 (2011) 305. https://doi.org/10.1557/opl.2011.799.

[7] H. Huisman, R. Ackermann, L. Claes, L. van Eijck, T. de Groot, I. Joosten, F. Kemmers, N. Kerkhoven, J.-W. de Kort, S. Lo Russo, D. Ngan-Tillard, B. van Os, M. Peter, C. Pümpin, J. Vaars, Z. Zhou, Change lost: Corrosion of Roman copper alloy coins in changing and variable burial environments, Journal of Archaeological Science: Reports. 47 (2023) 103799. https://doi.org/10.1016/j.jasrep.2022.103799.

[8] J.K. Fink, Chemicals and Methods for Conservation and Restoration: Paintings, Textiles, Fossils, Wood, Stones, Metals, and Glass, John Wiley & Sons, 2017.

[9]   L. Berriat, La Prassi Conservativa Per Le Monete "Archeologiche," Bollettino della Soprintendenza per i beni e le attività culturali della Valle d'Aosta. (2005) 171–172.

[10] G.V. Foster, J.D. Macisaac, Application of Xeroradiography to the Study of Bronze Coin(News and Short Contributions), Journal of Field Archaeology. 16 (1989) 245–255. https://doi.org/10.2307/529895.

[11] C. Sease, First Aid Treatment for Excavated Finds, in: Conservation on Archaeological Excavations, ICCROM, Italy, 1995: pp. 29–46. https://www.iccrom.org/publication/conservation-archaeological-excavations-particular-reference-mediterranean-area (accessed November 25, 2022).

[12] C. Sease, A Conservation Manual for the Field Archaeologist, 1994. https://escholarship.org/uc/item/8ft6488x (accessed January 18, 2023).

[13] R. Grayburn, M. Dowsett, M. Hand, P.-J. Sabbe, P. Thompson, A. Adriaens, Tracking the progression of bronze disease – A synchrotron X-ray diffraction study of nantokite hydrolysis, Corrosion Science. 91 (2015) 220–223. https://doi.org/10.1016/j.corsci.2014.11.021.

[14] D.A. Scott, Bronze Disease: A Review of Some Chemical Problems and the Role of Relative Humidity, (1990) 14.

[15] E. Ghey, Coin hoards and the Treasure process at the British Museum, in: EUT Edizioni Università di Trieste, 2019. https://www.openstarts.units.it/handle/10077/24663 (accessed January 3, 2023).

[16] D.M. Chico, Los tesoros imperiales de Hispania, Ph.D. thesis, Universitat de València, 2020. https://dialnet.unirioja.es/servlet/tesis?codigo=283410 (accessed January 9, 2023).

[17] S. Garraffo, Il Tesoro monetale di Suq el Kedim (Misurata, Libia), in: Il Tesoro Di Misurata (Libia) : Produzione e Circolazione Monetaria Nell'età Di Costantino Il Grande, Edizioni del Prisma, 2015: pp. 41–70. https://www.torrossa.com/en/resources/an/4855593 (accessed January 9, 2023).

[18] P.-M. Guihard, G. Blanchet, D'une perspective à l'autre. Le dépôt monétaire de ca 14500 nummi constantiniens découvert à Saint-Germain-de-Varreville (Manche, France), in: B. Callegher (Ed.), Too Big to Study? Troppo Grandi Da Studiare?, EUT Edizioni Università di Trieste, 2019: pp. 259–279. https://hal.archives-ouvertes.fr/hal-02146483 (accessed January 9, 2023).

[19] A. Stella, Too big to study? The numismatic collection in the National Museum of Aquileia, in: Too Big to Study? Troppo Grandi Da Studiare?, EUT Edizioni Università di Trieste, 2019. https://www.openstarts.units.it/handle/10077/24662 (accessed January 3, 2023).

[20] B. Bozzini, A. Gianoncelli, C. Mele, A. Siciliano, L. Mancini, Electrochemical reconstruction of a heavily corroded Tarentum hemiobolus silver coin: a study based on microfocus X-ray computed microtomography, Journal of Archaeological Science. 52 (2014) 24–30. https://doi.org/10.1016/j.jas.2014.08.002.

[21] M. Hess, L.W. MacDonald, J. Valach, Application of multi-modal 2D and 3D imaging and analytical techniques to document and examine coins on the example of two Roman silver denarii, Heritage Science. 6 (2018) 5. https://doi.org/10.1186/s40494-018-0169-2.

[22] G.T. Ingvardson, D. Müter, B.P. Foley, Purse of medieval silver coins from royal shipwreck revealed by X-ray microscale Computed Tomography (μCT) scanning, Journal of Archaeological Science: Reports. 43 (2022) 103468. https://doi.org/10.1016/j.jasrep.2022.103468.

[23] J. Miles, M. Mavrogordato, I. Sinclair, D. Hinton, R. Boardman, G. Earl, The use of computed tomography for the study of archaeological coins, Journal of Archaeological Science: Reports. 6 (2016) 35–41. https://doi.org/10.1016/j.jasrep.2016.01.019.

[24] J.M. Warnett, M.A. Williams, A. Attridge, D. Mearns, J.P. Vieira, Investigation of artefacts retrieved from a shipwreck of Vasco da Gama using X-ray Computed Tomography, in: 2017 IEEE International Instrumentation and Measurement Technology Conference (I2MTC), 2017: pp. 1–6. https://doi.org/10.1109/I2MTC.2017.7969982.

[25] A.S. Machado, A.S.S. Silva, G.N. Campos, C.S. Gomes, D.F. Oliveira, R.T. Lopes, Analysis of metallic archaeological artifacts by x-ray computed microtomography technique, Applied Radiation and Isotopes. 151 (2019) 274–279. https://doi.org/10.1016/j.apradiso.2019.06.016.

[26] R.O. Bude, E.M.R. Bigelow, Nano-CT evaluation of totally corroded coins: A demonstration study to determine if detail might still be discernible despite the lack of internal, non-corroded, metal, Archaeometry. 62 (2020) 1195–1201. https://doi.org/10.1111/arcm.12589.

[27] A.C. Kak, M. Slaney, Principles of Computerized Tomographic Imaging, Society for Industrial and Applied Mathematics, 2001. https://doi.org/10.1137/1.9780898719277.

[28] P.J. Withers, C. Bouman, S. Carmignato, V. Cnudde, D. Grimaldi, C.K. Hagen, E. Maire, M. Manley, A. Du Plessis, S.R. Stock, X-ray computed tomography, Nat Rev Methods Primers. 1 (2021) 1–21. https://doi.org/10.1038/s43586-021-00015-4.

[29] L.A. Feldkamp, L.C. Davis, J.W. Kress, Practical cone-beam algorithm, J. Opt. Soc. Am. A, JOSAA. 1 (1984) 612–619. https://doi.org/10.1364/JOSAA.1.000612.

[30] R. Brancaccio, M. Bettuzzi, M.P. Morigi, F. Casali, L. Ragazzini, Image Quality and Dose Assessment in Inner Ear Computed Tomography Imaging With a Flat Panel–Based System, Journal of Computer Assisted Tomography. 39 (2015) 232. https://doi.org/10.1097/RCT.0000000000000176.

[31] R. Brancaccio, M. Bettuzzi, F. Casali, M.P. Morigi, G. Levi, A. Gallo, G. Marchetti, D. Schneberk, 3D tomographic reconstruction on HPC cluster of the Kongo Rikishi (Japanese wooden statue of the XIII century), in: 2010 17th IEEE-NPSS Real Time Conference, 2010: pp. 1–8. https://doi.org/10.1109/RTC.2010.5750470.

[32] E. Corni, L. Morganti, M.P. Morigi, R. Brancaccio, M. Bettuzzi, G. Levi, E. Peccenini, D. Cesini, A. Ferraro, X-Ray Computed Tomography Applied to Objects of Cultural Heritage: Porting and Testing the Filtered Back-Projection Reconstruction Algorithm on Low Power Systems-on-Chip, in: 2016 24th Euromicro International Conference on Parallel, Distributed, and Network-Based Processing (PDP), 2016: pp. 369–372. https://doi.org/10.1109/PDP.2016.60.

[33] J. Schindelin, I. Arganda-Carreras, E. Frise, V. Kaynig, M. Longair, T. Pietzsch, S. Preibisch, C. Rueden, S. Saalfeld, B. Schmid, J.-Y. Tinevez, D.J. White, V. Hartenstein, K. Eliceiri, P. Tomancak, A. Cardona, Fiji: an open-source platform for biological-image analysis, Nat Methods. 9 (2012) 676–682. https://doi.org/10.1038/nmeth.2019.

[34] A. Fedorov, R. Beichel, J. Kalpathy-Cramer, J. Finet, J.-C. Fillion-Robin, S. Pujol, C. Bauer, D. Jennings, F. Fennessy, M. Sonka, J. Buatti, S. Aylward, J.V. Miller, S. Pieper, R. Kikinis, 3D Slicer as an image computing platform for the Quantitative Imaging Network, Magn Reson Imaging. 30 (2012) 1323–1341. https://doi.org/10.1016/j.mri.2012.05.001.

[35] CoinArchives LLC, CoinArchives.com: Numismatic and Market Research for Coins and Medals, (2023). https://www.coinarchives.com/ (accessed January 23, 2023).

[36] D. Kurth, Wildwinds, (2009). https://www.wildwinds.com/ (accessed January 3, 2023).

[37] Numista, Numista, (2007). https://en.numista.com/ (accessed January 23, 2023).

[38] OCRE, Online Coins of the Roman Empire, (2010). http://numismatics.org/ocre/ (accessed January 23, 2023).

[39] RStudio Team, RStudio: Integrated Development for R, (2020). http://www.rstudio.com/.

[40] WildWinds Ltd., Wildwinds, (2009). https://www.wildwinds.com/ (accessed February 13, 2023).

[41] A. Savio, Monete romane, Jouvence, Napoli, 2014.

[42] R. Wolters, The Julio-Claudians, in: W.E. Metcalf (Ed.), The Oxford Handbook of Greek and Roman Coinage, Oxford University Press, 2012: p. 0. https://doi.org/10.1093/oxfordhb/9780195305746.013.0019.

[43] C. Canovaro, I. Calliari, M. Asolati, F. Grazzi, A. Scherillo, Characterization of bronze Roman coins of the fifth century called nummi through different analytical techniques, Appl. Phys. A. 113 (2013) 1019–1028. https://doi.org/10.1007/s00339-013-7730-3.

[44] L.H. Cope, Roman Imperial Silver Coinage Alloy Standards: The Evidence, The Numismatic Chronicle (1966-). 7 (1967) 107–131.

[45] L.H. Cope, The metallurgical development of the Roman Imperial coinage during the first five centuries A.D, doctoral, Liverpool John Moores University, 1974. https://doi.org/10.24377/LJMU.t.00005590.

[46] J.N. Barrandon, J.P. Callu, C. Brenot, The analysis of constantinian coins (a.d. 313-40) by non-destructive californium 252 activation analysis*, Archaeometry. 19 (1977) 173–186. https://doi.org/10.1111/j.1475-4754.1977.tb00196.x.

[47] P.-M. Guihard, G. Blanchet, A. Bocquet-Liénard, J.-C. Angélique, É. Liénard, M.-P. Bataillé, J. Dupré, J.-L. Gabriel, Appréhender le stock de métal monnayé au ive siècle après J.-C., ArcheoSciences. Revue d'archéométrie. (2018) 45–62. https://doi.org/10.4000/archeosciences.5826.

[48] S. Garraffo, A. Nicolosi, G. Pappalardo, L. Pappalardo, F.P. Romano, Proceedings of the 6th Symposium of the Hellenic Society for Archaeometry, University of Michigan Press, Ann Arbor, MI, 2016. https://doi.org/10.30861/9781407314303.

[49] G. Pappalardo, A. Esposito, G.A. Cirrone, G. Cuttone, S. Garraffo, L. Pappalardo, F. Rizzo, F.P. Romano, S. Russo, Effects of the behaviour of the proton-induced isotopes production on the analysis of ancient alloys, Nuclear Instruments and Methods in Physics Research Section B: Beam Interactions with Materials and Atoms. 266 (2008) 2286–2291. https://doi.org/10.1016/j.nimb.2008.03.074.

[50] S. Scrivano, R. Pliego, B. Gómez-Tubío, J. Moreno-Soto, E. García Vargas, M. Ángel Respaldiza, F. Chaves Tristán, An approach to the metallic composition of the Carthage mint coins from the tetrarchic hoard of Tomares (CA. 312 CE), Journal of Archaeological Science: Reports. 44 (2022) 103509. https://doi.org/10.1016/j.jasrep.2022.103509.

[51] G.F. Carter, H. Razi, Chemical Composition of Copper-Based Coins of the Roman Republic, 217-31 B.C., in: Archaeological Chemistry IV, American Chemical Society, 1989: pp. 213–230. https://doi.org/10.1021/ba-1988-0220.ch011.

[52] I. Calliari, M. Magrini, A. Zambon, P. Guerriero, R. Martini, Microstructural and compositional characterization of Roman coins, X-Ray Spectrometry. 28 (1999) 86–90. https://doi.org/10.1002/(SICI)1097-4539(199903/04)28:2<86::AID-XRS313>3.0.CO;2-B.

[53] M. Scuotto, C. Bassi, M. Lezzerini, E. Grifoni, S. Legnaioli, G. Lorenzetti, S. Pagnotta, V. Palleschi, X-ray fluorescence analysis on a group of coins from the ancient roman city of

Tridentum (Trento, Italy), X-Ray Spectrometry. 43 (2014) 370–374. https://doi.org/10.1002/xrs.2567.

[54] K. Lockyear, Coin Hoards of the Roman Republic Online, version X, (2013). http://numismatics.org/chrr/ (accessed January 9, 2023).

[55] Oxford University, Coin Hoards of the Roman Empire dataset, (2013). https://chre.ashmus.ox.ac.uk/ (accessed January 9, 2023).

[56] M. Cotte, P.-O. Autran, C. Berruyer, C. Dejoie, J. Susini, P. Tafforeau, Cultural and Natural Heritage at the ESRF: Looking Back and to the Future, Synchrotron Radiation News. 32 (2019) 34–40. https://doi.org/10.1080/08940886.2019.1680213.

[57] L. Robbiola, J.-M. Blengino, C. Fiaud, Morphology and mechanisms of formation of natural patinas on archaeological Cu–Sn alloys, Corrosion Science. 40 (1998) 2083–2111. https://doi.org/10.1016/S0010-938X(98)00096-1.

[58] M.T. Doménech-Carbó, F. Di Turo, N. Montoya, F. Catalli, A. Doménech-Carbó, C. De Vito, FIB-FESEM and EMPA results on Antoninianus silver coins for manufacturing and corrosion processes, Sci Rep. 8 (2018) 10676. https://doi.org/10.1038/s41598-018-28990-x.

[59] E.S. Hedges, D.A. Robins, Examination of Some Silver-Coated Roman Coins, The Numismatic Chronicle and Journal of the Royal Numismatic Society. 3 (1963) 237–240.

[60] K. Manukyan, C. Fasano, A. Majumdar, G.F. Peaslee, M. Raddell, E. Stech, M. Wiescher, Surface manipulation techniques of Roman denarii, Applied Surface Science. 493 (2019) 818–828. https://doi.org/10.1016/j.apsusc.2019.06.296.

[61] F.P. Romano, S. Garraffo, L. Pappalardo, F. Rizzo, In situ investigation of the surface silvering of late Roman coins by combined use of high energy broad-beam and low energy micro-beam X-ray fluorescence techniques, Spectrochimica Acta Part B: Atomic Spectroscopy. 73 (2012) 13–19. https://doi.org/10.1016/j.sab.2012.05.012.

[62] C. Vlachou, J.G. McDonnell, R.C. Janaway, Experimental investigation of silvering in late Roman coinage, MRS Online Proceedings Library (OPL). 712 (2002) II9.2. https://doi.org/10.1557/PROC-712-II9.2.

SUPPORTING INFORMATION

Sample	ID Numbers	Before cleaning		After cleaning		
		Diameter *mm*	Weight *g*	Diameter *mm*	Weight *g*	Thickness mm
A1	20.S239-2.2549	29.2	7.9	28.8	6.4	2.5
A2	20.S239-2.2565	22.6	3.5	22.9	2.9	3.5
A3	20.S239-2.2568	19.9	2.6	19.5	2.0	2.1
A4	20.S239-2.2569	16.2	1.4	16.4	1.3	1.6
A5	20.S239-2.140602	19.3	1.9	19.3	1.7	2.5
B1	20.S239-2.2496	20.6	2.0	20.6	1.8	1.7
B2	20.S239-2.2556	15.1	2.7	15.0	2.4	2.3
B3	20.S239-2.2560	25.8	8.8	26.3	8.3	3.0
B4	20.S239-2.140524	17.3	1.6	17.3	1.6	1.3
B5	20.S239-2.2501	27.7	8.7	25.9	7.5	3.8
C	20.S239-2.2555	31.4	28.4	31.9	27.9	5.0
D	582411	-	-	15.0	1.6	1.6

Table S1 Metrology of coins before and after their cleaning. Coin D was cleaned prior to the present study. Diameter and thickness are intended as maximum value of multiple taken with a digital calliper and are expressed in millimetres. Weight has been measured with a precision balance and is expressed in grams. Tolerances are ±0.5 mm and ±0.1 g, respectively.
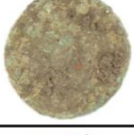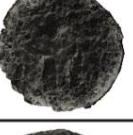
Sample		As-retrieved	XCT-based rendering	Cleaned
B1	*obv*			
	rev			
B2	*obv*			
	rev			
B3	*obv*			
	rev			
B4	*obv*			
	rev			
B5	*obv*			
	rev			

Figure S1 Group of five coins partially identified using XCT. Images display (from left to right, for each single row): coin as retrieved from the excavation site, 3D rendering based on tomographic reconstructions, coin after cleaning. 'obv' and 'rev' stand for obverse and reverse side. Images are not drawn to scale.

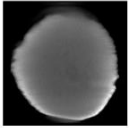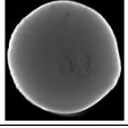| Sample		As-retrieved	Reconstructed slice	Cleaned
C	side A			
	side B			

Figure S2 Coin C, completely illegible under XCT. Images display (from left to right, for each single row): coin as retrieved from the archaeological site, a representative slice from the tomographic reconstruction, coin after cleaning. Side A and side B indicate the two faces of the coin, since the conservation state did not allow to recognise obverse and reverse.

Sample		As-retrieved	XCT-based rendering
D	obv		
	rev		

Figure S3 Single coin cleaned before tomographic analysis and revealing an 'S C' write on a side. (left) Optical photograph and (right) 3D rendering based on XCT data. 'obv' and 'rev' stand for obverse and reverse side. Images are not to drawn scale.

Figure S4 Graphical scheme of the µXCT setup used. From right to left: the HAMAMATSU X-ray source, the sample holder for the coins, placed on a rotating stage and held in vertical alignment by two blocks of polystyrene, and the VARIAN flat-panel detector.

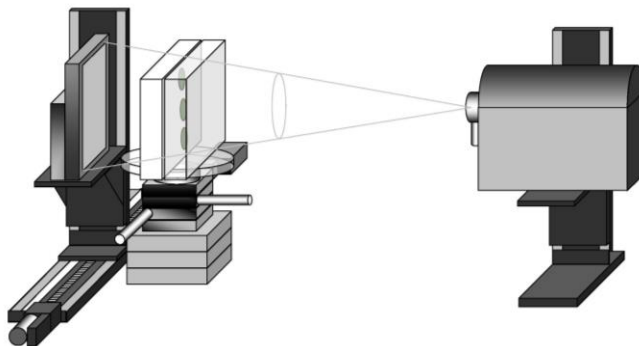| Sample	Reference data		Full numismatic legend	Photo with the permission of:
A1	**Maximianus** *Follis* (AE1) RIC VI 45b/47b Ticinum (300-303/304-305 CE)	*obv* *rev*	IMP C MA[XIMIANV]S PF AVG [SACRA MONET AVG]G ET CAES[S NOSTER]; exergue T$^?$[T]	wildwinds.com https://www.wildwinds.com/coins/ric/maximianus/_ticinum_RIC_045b.1.jpg
A2	**Valerianus I** *Antoninianus* RIC V.1 253 Milan (257-259 CE)	*obv* *rev*	IMP VALERIANVS P AVG SAL[VS A]VGG	wildwinds.com ex TimeLine Originals, June 2009 https://www.wildwinds.com/coins/ric/valerian_I/RIC_0253.jpg
A3	**Crispus Caesar** *Nummus* (AE3) RIC VII 132 Arles (317 CE)	*obv* *rev*	CR[ISPVS NOB CAES] [PRINCIPIA-IVV]ENTVTIS; exergue [QARL]; across the field [R]-S	wildwinds.com ex cng.fr, July 2001 https://www.wildwinds.com/coins/ric/crispus/_arles_RIC_132.jpg
A4	**Constans I** *Nummus* (AE3) RIC VIII 88A Siscia (337-341 CE)	*obv* *rev*	CO[NSTAN-S PF AVG] GLOR-IA-[EXERC-ITVS]; exergue ASIS$^?$	wildwinds.com ex ArtCoinsRoma, July 2012 http://www.wildwinds.com/coins/ric/constans/_siscia_RIC_viii_088.jpg
A4 (*O* mark)	**Constans I** *Nummus* (AE3) RIC VIII 77 Siscia (346-348 CE)	*obv* *rev*	CO[NSTAN-S MAX AVG] GLOR-IA-[EXERC-ITVS]; exergue ASIS$^?$	wildwinds.com August 2008 https://www.wildwinds.com/coins/ric/constans/_siscia_RIC_viii_077.jpg
A5	**Severus Alexander** *Denarius* RIC IV.1 92 Rome (229 CE)	*obv* *rev*	IMP SEV ALE-XAND AVG [PM TRP V]-III-C-OS III [PP]	wildwinds.com ex TimeLine Originals, July 2009 https://www.wildwinds.com/coins/ric/severus_alexander/RIC_0092.jpg

Table S2 Data of references used for coin identification in Fig.1, and related acknowledgments. Square brackets in legend description contain characters that are expected for the respective numismatic type, but not readable on the coin.

# Sample	Al	Si	P	S	Cl	Ca	Ti	Mn	Ni	Fe	Cu	Zn	Ag	Sn	Pb	Sum
A1	1.65 ± 0.09	0.10± 0.07	0.24± 0.08	0.8 ± 0.2	-	2.6 ± 0.9	0.13 ± 0.01	0.05 ± 0.03	0.02 ± 0.01	1.5 ± 0.2	62.6 ± 4.2	-	6.4 ± 1.1	12.2 ± 1.7	11.8 ± 2.1	100.10
A2	2.4 ± 0.2	1.3 ± 0.4	0.01 ± 0.01	0.29 ± 0.08	-	5.0 ± 2.4	0.22 ± 0.08	Trace	0.02 ± 0.01	0.49 ± 0.05	58.2 ± 12.4	-	31.8 ± 12.1	-	0.37 ± 0.06	100.10
A3	1.4 ± 0.2	0.6 ± 0.2	Trace	0.26 ± 0.08	0.5 ± 0.3	1.9 ± 1.0	0.14 ± 0.01	Trace	0.04 ± 0.01	0.28 ± 0.04	61.5 ± 6.8	-	2.4 ± 0.9	12.1 ± 1.9	19.0 ± 7.1	100.11
A4	1.4 ± 0.2	0.5 ± 0.3	Trace	-	-	0.8 ± 0.2	0.13 ± 0.01	-	0.06 ± 0.02	0.34 ± 0.08	56.1 ± 7.2	-	2.0 ± 0.5	12.6 ± 2.0	26.2 ± 5.4	100.13
A5	3.0 ± 0.2	0.5 ± 0.1	0.05 ± 0.03	1.7 ± 0.2	-	0.7 ± 0.2	0.12 ± 0.01	-	0.03 ± 0.01	0.14 ± 0.04	46.1 ± 3.4	-	47.5 ± 3.1	-	0.26 ± 0.08	100.10
B1	1.49 ± 0.09	0.36 ± 0.09	0.16 ± 0.03	-	-	1.0 ± 0.2	0.12 ± 0.01	0.04 ± 0.01	0.03 ± 0.01	1.5 ± 0.2	66.1 ± 2.6	-	5.3 ± 0.9	18.6 ± 1.9	5.4 ± 0.9	100.10
B2	1.0 ± 0.1	0.33 ± 0.1	0.7 ± 0.2	0.09 ± 0.02	-	0.96 ± 0.09	0.10 ± 0.01	0.01 ± 0.01	0.03 ± 0.01	0.9 ± 0.2	61.2 ± 2.0	0.07 ± 0.02	0.15 ± 0.01	25.6 ± 1.7	9.0 ± 0.4	100.14
B3	2.10 ± 0.05	0.30 ± 0.06	0.05 ± 0.01	0.09 ± 0.01	-	0.5 ± 0.2	0.10 ± 0.01	0.02 ± 0.01	Trace	0.23 ± 0.05	96.6 ± 0.2	-	-	-	-	99.97
B4	1.63 ± 0.05	0.02 ± 0.02	0.10 ± 0.02	-	-	0.53 ± 0.03	0.12 ± 0.01	0.01 ± 0.01	0.05 ± 0.01	0.05 ± 0.01	69.3 ± 0.8	-	-	-	28.2 ± 0.8	100.02
B5	1.93 ± 0.08	0.8 ± 0.4	0.15 ± 0.06	1.5 ± 0.6	-	0.4 ± 0.1	0.11 ± 0.01	Trace	Trace	0.16 ± 0.04	95.0 ± 1.1	-	-	-	-	100.04
C	1.5 ± ± 0.1	0.9 ± 0.2	-	0.11 ± 0.03	-	1.6 ± 0.3	0.18 ± 0.01	Trace	0.02 ± 0.01	2.4 ± 0.6	67.0 ± 4.1	-	-	18.4 ± 1.3	7.9 ± 2.7	100.02
D	2.4 ± 0.1	2.1 ± 0.4	0.10 ± 0.01	-	-	1.2 ± 0.2	0.15 ± 0.01	0.01 ± 0.01	0.01 ± 0.01	1.2 ± 0.2	92.8 ± 0.9	-	-	-	-	99.97

Table S3 Semi-quantitative results from XRF analysis, in wt%. Each measurement has been conducted in triplicate on each side of coins, at different spots. The results shown are the mean of the six measurements, normalised to 100%. The error is estimated as the standard deviation of the mean. For all the coins, Al, Si, Ca, Ti, Ni and Fe were detected and considered as soil contamination or part of corrosion compound. The same applies to traces of Mn, P and Cl occasionally found. Elements marked as 'Traces' are visible in the XRF spectrum, but quantification results lead to values lower than 0.01.

APPENDIX A: Beam hardening artefacts and correction

Beam Hardening (BH) is a physical phenomenon that occurs in X−ray imaging when the X-ray tube emits a multi-energy beam. When X-rays of different energies pass through an object, particularly for high-density materials and when thickness is significant, low-energy photons are more easily absorbed than high-energy photons, causing an increase in the average energy of the beam. This effect is known as 'beam hardening'. For a polychromatic X-Ray beam, the attenuation values deviate from a pure logarithmic function of the absorber's thickness (Lambert-Beer law). As a result of this phenomenon, with filtered back-projection algorithms, the reconstructed slices will have CT values gradually decreasing from the edges toward the center even in the case of an object with uniform density, resulting in a 'cupping artifact' [1]. Furthermore, the tomographic images lose contrast and some object details are not clearly visible.

BH is a well-known phenomenon in computed tomography and is generally corrected by means of a calibration procedure which requires the creation of an *ad hoc* phantom for each type of experiment/material [2–4] or by post-processing correction [5]. The second approach has been followed in this work. Furthermore, to physically limit the phenomenon, filters have been applied in front of the X−ray tube window as described in the previous section.

Beam hardening has been observed in all the tomographic reconstructions. In our case, beam hardening prevented the retrieval of any kind of information from the core of the objects. Despite this, the outer surface of the coin was always visible in the tomographic reconstructions, except for the case of coin C (Fig. S2). The presence of beam hardening possibly indicates that the coins have residual metallic bulk within.

After the application of the BH correction, the contrast increases, highlighting, thus, the lettering along with other details. Fig. S5 reports an example of the effects of the BH correction on the dataset. In order to quantitatively evaluate these effects, the contrast at the two opposite sides of the emperor head has been calculated before and after the application of BH correction, using the following expression:

$$C = \frac{L2 - L1}{L2 + L1}$$

where L1 and L2 are the intensity values at the selected points along the intensity profiles shown in Fig. S5b. A contrast increment of 15% (red ROI) and 20% (yellow ROI) can be observed.
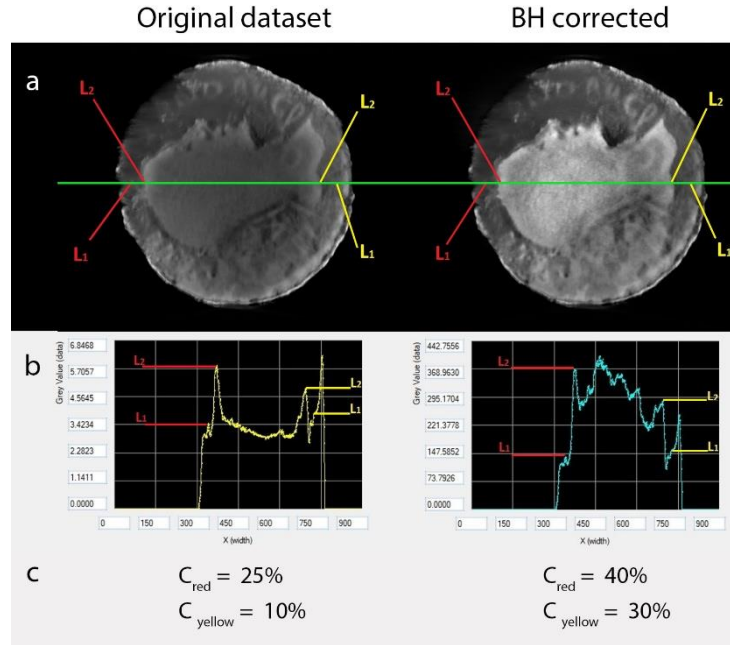
Figure S5 Example of the effects of BH correction on coin A5 (obverse). In Fig. S5a, two corresponding slices from the original dataset (left) and from the BH corrected one (right) are reported. The green line indicates localization where the intensity profiles (shown in Fig. S5b) are taken. L1 and L2 markers of corresponding colors indicate, in both slices and intensity profiles, the same pixels, which have been used for the calculation of the contrast reported in Fig. S5c.

APPENDIX B: Image processing steps

Full-scan datacubes have been first reconstructed from µXCT scans and then corrected for beam hardening. BH-corrected data subsequently underwent only basic post-processing steps. First, each datacube (including the scans of 2-3 coins) has been split into one datacube per coin. Second, slight angular corrections have been applied to each coin-datacube (using the 'Reslice' and 'Rotate' commands in ImageJ). This step allowed to align the coin faces perpendicularly to the slicing direction. As shown in Fig. S6, it proved to be particularly helpful in enhancing features extraction. When the obverse and the reverse side of a coin showed two different angular orientations, the operation has been conducted twice, generating two distinct datacubes, one per face.
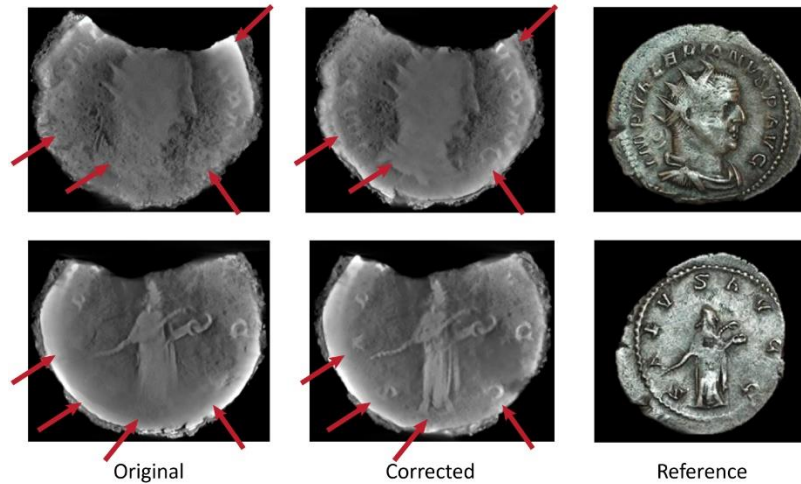
Figure S6 Example of a slice from the tomographic reconstruction of coin A2 to highlight the effect of angular correction on its readability: original (left), after correction (middle), and reference image (right). Obverse (top) and reverse (bottom) are both provided. Red arrows indicate major changes following angular correction.

Fig. S7 shows the cross-sectional views of a coin from one of such datacubes. Even if a minimum in the intensity histogram can be observed, segmentation by global thresholding from such distribution provided only limited results. All other coins showed a similar behaviour.
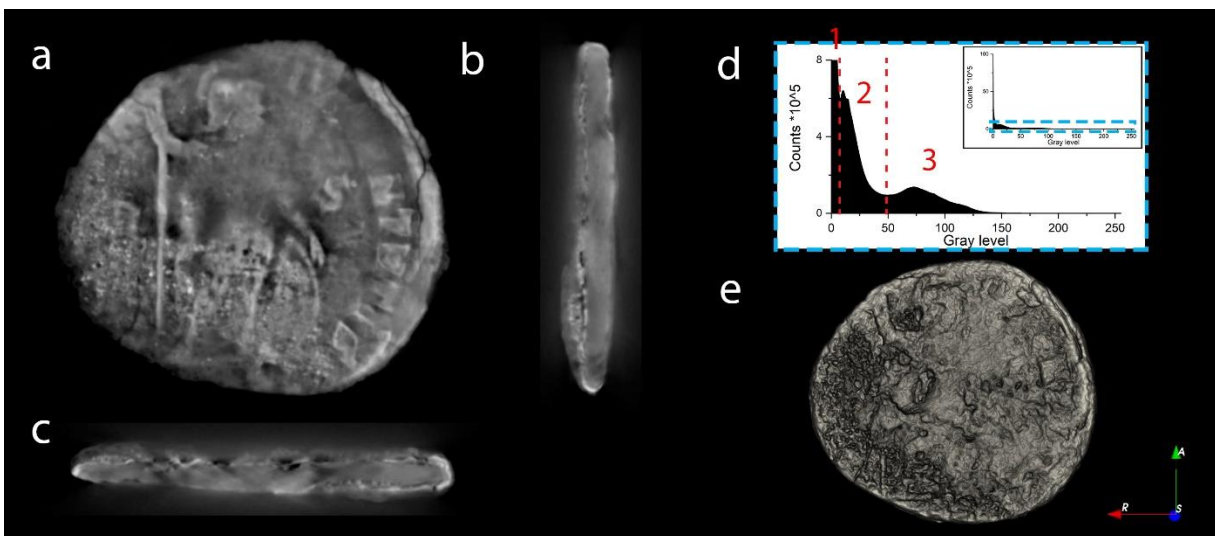

Figure S7 a) Slice from the reverse side of coin A3. b) and c) cross-sectional views of the coin. d) Intensity histogram of the full datacube. Onset: full scale histogram. Main figure: zoom on the lower zone. Region marked with '1' is linked to noise. e) 3D volume rendering after segmentation by global thresholding at the minimum between regions '2' and '3' in the histogram d), considering only the pixels above this threshold.

The complete extraction of information for coins identification has been performed from the so-processed datacubes by dynamically navigating through slices (i.e. CT sections). This procedure has been complemented with the generation of images through the application of basic math operations (average,

median, standard deviation, sum, maximum or minimum intensity) to neighbour slices, using the 'Z project' command in ImageJ, helpful in emphasising specific details.

In the case of coin A4 (Fig. 2), a low-pass filter has been further used in order to remove higher frequency features, correlated to noise and corrosion, and enhance the reading of the mark on the banner. It has been applied through the ImageJ command 'bandpass filter', setting the filtering range from 0 to 5 pixels.

The latter represents the only case in which an elaboration step, additional to angular correction and basic math operations, was needed. Further elaborations, such as image filtering, have been attempted on all coins, but they did not led to the discovery of any further information. The reason is that the complete extraction of any surviving detail from the original surface of the coins was already achieved after the basic steps listed before, as can be observed from the comparison between 3D renderings and physically cleaned coins in Fig. 1 and Fig. S1. For such reason, all the images reported in the manuscript come from unfiltered data (excepting Fig. 2C).

3D renderings have been performed with the support of 3D Slicer software. Volume renderings have been created using the processed datacubes as a whole. For achieving the images reported in the present work, a combination of thresholding and contrast management (through the 'Shift' command), virtual slicing (through the 'ROI' command) and lighting management (through the 'Light' Module) has been used. In this work, renderings have been mostly employed for communication purposes. In fact, only 3D renderings allowed for the display of all the details of a coin side and thus for summarising the results obtained in a single, static image. However, 3D renderings may also support the extraction of information, in particular thanks to the dynamic lighting capabilities, and they also open the way to a plethora of further applications, from virtual cleaning to digital twinning.

References

[1]   P.J. Withers, C. Bouman, S. Carmignato, V. Cnudde, D. Grimaldi, C.K. Hagen, E. Maire, M. Manley, A. Du Plessis, S.R. Stock, X-ray computed tomography, Nat Rev Methods Primers. 1 (2021) 1–21. https://doi.org/10.1038/s43586-021-00015-4.

[2]   J. Hsieh, Computed Tomography: Principles, Design, Artifacts, and Recent Advances, John Wiley & Sons, 2009. https://www.wiley.com/en-us/Computed+Tomography+Principles%2C+Design%2C+Artifacts%2C+and+Recent+Advances%2C+2nd+Edition-p-9780470563533.

[3]   E. Van de Casteele, D. Van de Dyck, J. Sijbers, E. Raman, The effect of beam hardening on resolution in x-ray microtomography, in: Medical Imaging 2004: Image Processing, SPIE, 2004: pp. 2089–2096. https://doi.org/10.1117/12.535263.

[4]   C.H. Yan, R.T. Whalen, G.S. Beaupre, S.Y. Yen, S. Napel, Reconstruction algorithm for polychromatic CT imaging: application to beam hardening correction, IEEE Transactions on Medical Imaging. 19 (2000) 1–11. https://doi.org/10.1109/42.832955.

[5]   Zhao Wei, Fu Guo-Tao, Sun Cui-Li, Wang Yan-Fang, Wei Cun-Feng, Cao Da-Quan, Tang Xiao, Wei Long, Beam hardening correction for a cone-beam CT system and its effect on spatial resolution, Chinese Phys. C. 35 (2011) 978. https://doi.org/10.1088/1674-1137/35/10/018.